Research Square

Preprints are preliminary reports that have not undergone peer review.
They should not be considered conclusive, used to inform clinical practice,
or referenced by the media as validated information.

Hydrodynamic properties of plasmid DNA from physical and ionic treatment influence E. coli transform

Achilles Ereve Espaldon

aespaldon@usa.edu.ph

Center for Advanced New Materials, Emerging and Engineering Technologies (CANMEET), University of San Agustin https://orcid.org/0000-0002-5326-4312

Stephen G. Sabinay

West Visayas State University

Ignacio A. Catelo

Pamantasan ng Lungsod ng Maynila College of Medicine: University of the City of Manila College of Medicine

Noel Peter B. Tan

University of San Agustin

Research Article

Keywords: Antibiotic-resistant plasmid, horizontal gene transfer, hydrodynamic size, transformation, zeta potential

Posted Date: May 15th, 2026

DOI: https://doi.org/10.21203/rs.3.rs-9466360/v1

License: This work is licensed under a Creative Commons Attribution 4.0 International License.
Read Full License

Additional Declarations:
Table 1 is available in the Supplementary Files section.

Hydrodynamic properties of plasmid DNA from physical and ionic treatment influence *E. coli* transform

Achilles E. Espaldon [a, b, c] *, Stephen G. Sabinay [d], Ignacio A. Catelo [e], Noel Peter B. Tan [a, b]

[a] Center for Advanced New Materials, Engineering, and Emerging Technologies (CANMEET), University of San Agustin, Iloilo City, Philippines

[b] Department of Chemical Engineering, University of San Agustin, Iloilo City, Philippines

[c] Gregor Mendel Research Laboratories, University of San Agustin, Iloilo City, Philippines

[d] West Visayas State University, Iloilo City, Philippines

[e] Department of Human Anatomy, Pamantasan ng Lungsod ng Maynila, Intramuros, Metro Manila, Philippines

* Corresponding author:

Achilles E. Espaldon

Mailing address:

Center for Advanced New Materials, Engineering, and Emerging Technologies (CANMEET), University of San Agustin, 5000 General Luna St.

Iloilo City, Philippines

E-mail: aeespaldon@gmail.com

Highlights

- Treatment-based variations of plasmid DNAs is detected by hydrodynamic properties and fluorescence which may occur in the aqueous environment
- Transformation efficiency of plasmid-encoded ARGs in *E. coli* is influenced by the hydrodynamic properties for a higher-molecular weight plasmid
- The Mg^{2+} cations reduces the zeta potential of the plasmid and which indicates aggregation and condensation

Abstract

Antibiotic resistance emerges when multidrug-resistant plasmid DNA is transferred via horizontal gene transfer (HGT) into viable bacterial hosts. In aquatic environments, plasmid DNAs can undergo hydrodynamic and structural variations due to physicochemical influences, which may affect the efficiency of gene transfer. This study investigates the effects of bead beating (BB) as a physical treatment and magnesium ion (Mg^{2+}) treatment on plasmids pBR322 (4.6 kb) and RP4 (60 kb) in water. Treated plasmids were characterized by fluorescence spectrophotometry, hydrodynamic size, and zeta potential, and subsequently transformed into competent *Escherichia coli* DH5α. Denaturation by bead beating increased the hydrodynamic size and reduced the zeta potential of the larger RP4 plasmid, which followed a decreased transformation efficiency. Conversely, Mg^{2+} ions induced plasmid aggregation and concentration-dependent charge neutralization, enhancing plasmid re-uptake efficiency, which was significantly observed at 100 mM. These findings emphasize that plasmid size, structure, and electrostatic interactions influence the potential for gene transfer in aquatic environments.

Keywords and Speciality: Antibiotic-resistant plasmid, horizontal gene transfer, hydrodynamic size, transformation, zeta potential

1. Introduction

Antibiotic resistance (ABR) is now a significant global health concern, largely driven by the dissemination of antibiotic-resistant genes (ARGs). ARGs have emerged as important biological contaminants in aquatic environments (Amarasiri et al. 2019; Wang et al. 2022). These genes spread among microorganisms primarily via horizontal gene transfer (HGT) of plasmid DNAs (pDNAs) which mediate in all major HGT mechanisms: transformation, conjugation, and transduction (von Wintersdorff et al. 2016).

In essence, ARGs or plasmid-encoded ARGs pose a direct health risk only when present in viable pathogenic hosts capable of causing infection (Manaia 2017). Extracellular ARGs are commonly found in the environment as genetic material, but non-viable or inactivated microorganisms cannot express resistance or participate in HGT. However, intact extracellular pDNAs or ARGs released into the environment can be taken up by viable pathogens through transformation, which enables the reintegration of resistance traits. Therefore, understanding transformation-mediated gene transfer is essential to assess the true risk of ARG contamination.

It has been established that DNA size by base pair length negatively correlates with transformation frequency in *E. coli* (Hanahan 1983; Szostková and Horáková 1998). Plasmid conformations exist as topoisomers such as supercoiled/covalently closed circular (SC/CCC), relaxed open circular (OC), and linear (L) forms (Huang and Chen, 1990). Hanahan (1983) reported no significant transformability differences among these forms with similar base pairs. Other work reported higher transformation efficiency of SC plasmids compared to denatured OC and linear forms. However, these studies often used different hosts, such as *B. subtilis* or various mammalian cell lines, that may differ significantly in transformation mechanisms from *E. coli* (Cherng et al. 1999; Ohse et al. 1997; Demaneche et al. 2002; Guragain et al. 2024).

In aquatic environments, pARGs may exist in various structural conformations. This reflects the pDNA's intrinsic ability to adopt different forms *in vivo* (Bochman et al. 2012). One possible fate of plasmids in water is denaturation via loss of supercoiling, often caused by shearing forces that reduce superhelicity, induce denaturation, or cause strand breakage (Levy et al. 1999; Hershey et al. 1963). Additionally, pDNA's highly negative charge allows interactions with cations in water, such as divalent Ca^{2+} and Mg^{2+} ions, which can promote cell competence, reduce electrostatic repulsion, and induce compaction or condensation of extracellular DNA

(Zinchenko et al. 2009). These potential structural implications are still limited under the current HGT understanding of ABR.

Furthermore, most earlier studies used idealized DNA topologies produced by enzymatic treatments. Topoisomerases induce relaxation to OC form while restriction enzyme causes linearization of pDNAs. However, these may not reflect the actual alterations in pDNAs, as probabilities may be low and unlikely to occur in the natural aquatic environments. The abundance of cations in water, as it reflects *in vivo*, as well as the physical stresses in water streams, may better simulate environmental HGT phenomena.

Interestingly, no studies so far have considered and characterized the hydrodynamic and structural properties of pDNAs with respect to their probability of transformation. It would be important to determine what hydrodynamic and structural features of the pDNAs, by physico-chemical treatment, may affect their transformability. Such understanding may offer new insights and reveal new challenges in HGT in the spread of ABR, particularly in the aquatic environment.

Based on this discussion, this study aimed to characterize the patterns in the hydrodynamic properties of size, zeta potential, and structure of multidrug-resistant plasmid DNA following physico-chemical treatment. BB-treated pDNA was vortexed with beads, while MT-pDNA was treated with increasing concentrations of Mg^{2+}. Then, the effect of these treatments was evaluated on plasmid transformability in *Escherichia coli.* Bacterial transformation was performed via the heat shock approach for two sizes of plasmids, the smaller pBR322 plasmid and the larger RP4 using a calcium-induced competent *E. coli* DH5α as host. Transformants were selected with ampicillin (both pBR32 and RP4) and kanamycin (RP4 only) antibiotics.

2. Methods and Materials

2.1 Preparation of competent cells

A 5 mL of LB (Lennox) broth was inoculated by picking a single, isolated colony from an overnight streaked LB agar plate, then incubated at 37°C for 8-10 hr. to the stationary phase. Then, 500 μL (1:10) of this *E. coli* culture was transferred into an LB broth, now at 1:100 dilutions, and incubated for 4 hrs. to reach mid-exponential phase at *ca.* 5-8 x 10^7 CFU/ml or with an optical density of OD600 at 0.4–0.6. The *E. coli* cells were then centrifuged at

8,000 rpm for 5 min at 4°C. The supernatant was discarded, and pellets were washed twice with phosphate buffer solution (pH 7). Thereafter, the pellets from the second washing were gently resuspended in ½ volume of ice-cold 30 mM $CaCl_2$ and incubated for 1 hour at 4°C. Then, the suspension was centrifuged again using the same parameters and resuspended in the same salt solution to a final concentration of 1/10 of the volume. This resuspension of competent cells of around 4 mL was immediately used for the transformation.

2.2 Plasmid extraction and stock preparation

Plasmids were extracted using a commercially available plasmid extraction kit (Qiagen Mega and Maxi Prep), following the manufacturer's instructions. The extracted plasmids were eluted in 10 mM Tris-HCl buffer (pH 8.5) in 50 µL aliquots and stored at -20°C. The purity and concentration of the extracted plasmids were determined using a NanoDrop spectrophotometer (Thermo Fisher Scientific) with A260/280 >1.8 and A260/230 > 2.0. The absorbance ratio of A260/280 is roughly 1.8, indicating an acceptable purity of the extracted plasmid. The concentration of the plasmid stock solution is about 200 – 400 ng/µL from various extraction batches.

2.3 Plasmid treatment

Concentrations of plasmid RP4 for the particle size analysis and zeta potential (PSA-ZP) were prepared from stock solutions to 120 and 17 ng/μL using Milli Q water. Untreated plasmid, N, was prepared from the stock plasmid concentration extracted in TE buffer (pH 8) while addition of an appropriate volume from stock solutions of $MgCl_2$ (200 mM) for MT-pDNA achieved final concentrations of 1, 3, 5, 10 and 100 mM. Stock solutions of $MgCl_2$ filtered using 0.22 µm membrane filter and were cleaned by injecting around 10 mL of Milli-Q water.

For the preparation of plasmid samples prior to transformation, the previously described steps for the PSA-ZP sample preparation were conducted except that the final concentration was 1.88 ng/µL for RP4 and 10.0 ng/µL for pBR322. To generate the denatured plasmid, a 4-mm. Glass/ meta bead (Lysing Matrix E, MP Biomedicals) is placed in the 1.5 mL microfuge containing the N sample plasmid and vortexed using Vortex-mini 2 at high speed for 5-, 10-, and 20-min. Thereafter, the glass bead was removed by a pair of tweezers prior to transformation. Hereafter, denaturation by bead beating is referred to as BB-pDNA. All plasmids treated with Mg^{2+} are referred to as MT-pDNA, and for 10 mM addition, as an example, referred to as MT-10.

2.4 Fluorescence spectrophotometry

Following the plasmid's treatment described in 2.3, fluorescence spectra of the pBR322 plasmid were recorded using a fluorescence spectrophotometer (Cary Eclipse Agilent 9802). SYBR green (SG) safe (Invitrogen, Japan) solution was diluted to 1:4500 in Milli Q water. After treatment, 3mL of the samples at roughly 17 *n*g/µL were added with 2 mL of SG solution and incubated for 5 min, at room temperature. The plasmid-SG mix was added to the 3 mL rectangular quartz cuvette at 10mm path length. Excitation was conducted at 502 nm with an emission at 530 nm. In another test, the same plasmid's fluorescence was measured from the Victor Nivo multimode plate reader (Perkin Elmer). pBR322 samples at around 1.5 ng/µL were added with a 1.25:1 volume ratio of QuantiFluor ONE dsDNA Dye (Promega), where the latter was prepared at a 1:450 dilution from its stock dye concentrate. After 5 min. After incubation, endpoint fluorescence emission was measured at 530 nm wavelength with triplicate readings.

2.5 Hydrodynamic size analysis by dynamic light scattering

The hydrodynamic diameter was measured using the single-angle dynamic light scattering (DLS) method at 25°C and analyzed by autocorrelation function and using the photon correlation spectroscopic principles (Malvern Zetasizer, Malvern Panalytical Ltd., Japan). All samples were prepared in a cellulose-membrane-filtered 5 mM NaCl solution, at a concentration of 120 ng/μL and 17 ng/μL for RP4. All experiments were carried out with filtered Milli Q water as the dispersant. The DTS1070 cell (Malvern Panalytical Ltd., Japan) was used in all the measurements and was washed twice with filtered Milli-Q water. Samples were injected at 750 μL, and the temperature was set to 25 °C, and the viscosity at 0.8872 cP. Protein was used as the model refractive index at 1.333. All samples were tested first with the size and subsequently, the zeta measurement. The size in the form of the hydrodynamic radius is derived from the diffusion coefficient as shown in Eqn. 4.1 is known as the Stokes-Einstein equation.

$$D = \frac{k_B . T}{6.\pi.\mu.R_H} \qquad \text{(Eqn. 1)}$$

Where D Is the diffusion coefficient, k_B Is the Boltzmann constant, T Is the temperature, μ Is the fluid's viscosity, and R_H, as the hydrodynamic radius. In the DLS Malvern Zetasizer, the size distribution x-axis plot is labelled

d.nm, which reads the hydrodynamic diameter in nm. Both the size distribution by intensity and number were used to assess the patterns of hydrodynamic size changes.

2.6 Zeta potential analysis

Zeta (ζ) potential measurements of the RP4 plasmid (60 kbp) were conducted using the Malvern Zetasizer Ultra equipment (Malvern Panalytical Ltd., Japan). All samples were prepared similarly to the hydrodynamic size measurement via DLS (Section 2.5). Auto mode was used as the data processing analysis model. For the calculation of the ξ potential, Henry's equation (Eqn. 2) was used to calculate the zeta potential.

$$U_e = \frac{2.\varepsilon.\xi.f(ka)}{3.\mu} \qquad \text{(Eqn. 2)}$$

Where U_e Is the electrophoretic mobility, ε, is the dielectric constant, ξ as the zeta potential, f(ka) Is Henry's function, with k as the inverse Debye length, λ_D, a as the molecular radius, and μ Is the fluid's viscosity.

2.7 Bacterial transformation

A 200 μL of a competent *E. coli* suspension was added with 100 μL of the plasmid-treated (BB, N, MTs) solution in a 1.5 mL microcentrifuge tube, and the transform mix was incubated for 30 min. on ice for pBR322 and 60 min. for the RP4 plasmid. The transform mix involving the RP4 plasmid was added with 4 μL of 80% w/w PEG-8000. Then, the mixture was heat-pulsed at 42°C in a water bath for 45 seconds. For pBR322 and 2 min. for RP4, and thereafter, incubated again on ice for 2 min. for recovery. Then, super-optimal broth with glucose (SOC) medium was added and incubated for 45 min. At 37°C in a shaker at 120 RPM (Hanahan et al., 1991). The transform mix was serially diluted in 1.5 microcentrifuge tubes and plated with 500 µL on LB agar supplemented with 60 μg/mL of ampicillin (for pBR322 only) and 25 μg/mL of kanamycin. Transformants were enumerated after incubation for 21–24 hr. at 37 °C. Transformation gene transfer was quantified using transformation efficiency (TE), as the number of viable transformants per amount of plasmid (Eqn. 3). The lower limit of detection for the plating assay is 1 transformant CFU/mL or a no-detection result as 0 CFU/mL.

$$\text{Transformation efficiency} = \frac{\text{Transformants}, \frac{\text{CFU}}{\text{mL}}}{\text{amount of plasmid, ug}} \qquad \text{Eqn. (3)}$$

2.8 Statistical analysis and post-processing software

GraphPad Prism (http://www.graphpad.com/) and SocSci statistics (https://www.statskingdom.com) were used for the ANOVA with Tukey HSD, respectively. The *p*-value of 0.05 was employed in all the other statistical tests. All graphs were constructed using the Veusz plotting software. Grammarly (Grammarly Inc.) was used as an AI-powered writing assistant to check and correct the grammar but was not used to change the writing context or increase the writing overall score.

3. Results and Discussions

3.1 Fluorescence spectrophotometry

To determine the effect of the plasmid treatment on the structure, fluorescence spectra were recorded as shown in Fig. 1(a) tested for the pBR322 (4.3 kb) only. Fluorescence was emitted with SYBR green (SG) dye staining and with the formation of the SG-plasmid DNA complex after excitation at 502 nm (not shown) and emission at 530 nm (SYBR green safe). The dye is used as a probe, and the fluorescence significantly increases when it is bound to DNA. Emission at 530 nm shows N as the reference intensity relative to BB and MT-1 to MT-5. In a separate fluorescence test (end-point fluorescence) on the peak emission at 530 nm (Fig. 1b), a minimal 1.4% decrease in intensity was observed in BB denaturation, while a relatively higher intensity reduction was achieved at 50.4% maximum at MT-10. Although the fluorescence spectra were tested on a different concentration ranges with slight differences compared to 530 nm end-point emission (test limitation), a concentration-dependent decrease in fluorescence intensity pattern was observed in the MTs.

The fluorescence spectrophotometry is a sensitive method to detect the changes and patterns in molecular structures by means of the emitted fluorescence as a result of the differential binding of a dye (Krause et al. 2000). Fluorescence intensity is related to the bound ligand (dye) in the equation, $I = \alpha \cdot c_{DNA} \cdot N_{bound}$, where α is a proportionality factor that depends on the dye quantum yield, c_{DNA}, as the concentration of the DNA and N_{bound},

as the no. of bound dye molecules. The significant differences in the fluorescence emissions (Fig. 1b) indicates that the treatment of the pDNAs affected the dye binding and are considered as distinct forms as compared to N-pDNA.

Fig. 1 (a) Fluorescence spectra of pBR322 upon treatment (b) End-point fluorescence emission at 530 nm (n = 3). Significant difference by independent sample t-test and one asterisk (*) indicates p value < 0.05 (n = 3). Error bar (not seen due to minimal deviation relative to intensity) is one standard deviation.

SG dye has two functional groups that bind to dsDNA; the quinolinium-thiazole aromatic group intercalates between DNA base pairs and its aminopropyl moieties, having the positive charge, interact with the minor groove of the negative-bearing sugar-phosphate group of the plasmid (Dragan et al. 2012). The structural stability of double-stranded DNA depends on the integrity of its sugar-phosphate backbone. Hence, any disruption or changes to the backbone may affect the binding of the dye which leads to the reduction of fluorescence.

The untreated N-pDNA for pBR322, previously characterized to exhibit a single band, supercoiled form (Fig. S1, Lane 7) and with a higher intensity than the BB-pDNA indicates a reduced supercoiling in the BB-treated and as detected from previous works (Hahn 2025; Kolbeck et al. 2023; Sandhu et al. 1985; Zipper et al. 2004). Upon response to shearing and in similar physical denaturation treatment, it is expected that changes would be minimal by less than a 2-fold change and agrees well with a previous study (Shapiro et al. 2010). Shapiro and others (2010) reported that shearing is less sensitive to smaller plasmid sizes. Around 2-3% (estimated) reduction in supercoiling was also observed at a shear rate of $3.5 \times 10^5\ s^{-1}$ for a plasmid size of 13 kb (in this case the pBR322 at 4.3 kb is even less) (Levy et al. 1999). Some damage in a double stranded gene fragment when denatured by thermal and chemical treatment would also reduce the fluorescence intensity and can be detected by a similar capillary gel electrophoresis (Agilent bioanalyzer) (Wang et al. 2022). Lastly, the local structural transition in DNA from the B-type into its Z-type isomer, which is a stretched version of the native type, is also manifested by loss of fluorescence (Hur et al. 2019; Nial and Subudhi 2024) yet may only be inferred to have occurred in the BB treatment due to a lack of other spectroscopic tools (*e.g.* circular dichroism).

The similar effect on the MT-pDNAs, although higher in % reduction than BB-treated, has also affected the binding of the SG dye. Mg^{2+} typically binds both to the major and minor groove of the sugar-phosphate backbone which may bind competitively (as being added first prior to the dye) with the SG binding (Georgiou and Papapostolou 2006; Guéroult et al. 2012b; Nath et al. 2000). It should be noted that Mg^{2+} was added prior to the dye intercalation, hence the effect on fluorescence from any potential change in structure was caused by Mg^{2+}, after which the dye would bind accordingly. Intramolecularly, cation addition may have also altered the plasmid's structure, either by bending or stretching (Rouzina and Bloomfield 1998) and a combination of aggregation and condensation (Tsoi et al. 2010). Lastly, Mg^{2+} binding may also promote formation of bundles, aggregates and other ordered structures because of the intermolecular attraction (Liu et al. 2011) and which may inhibit dye intercalation and binding.

3.2 Hydrodynamic diameter

The effect of the treatment was also reflected in the hydrodynamic sizes, or diameters, D_H. In Fig 2, the size distribution by number (SDN) shows the comparison of BB and MT-pDNAs as well as patterns of changes in their predominant sizes. In the SDN, all size distributions showed monomodal peaks. In the size distribution by intensity (SDI) (Table S1), the distribution demonstrated significant multiple modal peaks with large particle sizes even in the untreated sample (N). This may indicate presence of plasmid aggregates which may be formed due to the presence of salt from sample preparation (5 mM NaCl) and the high plasmid concentration. However, the peak for the smaller size particle is in good agreement with the expected rod-like or cylindrical helix with dimensions of width (not hydrodynamic width) and length (Folarin et al. 2019; Ke et al. 2010; Ledley 1996; Nayvelt I et al. 2007; Prevette et al. 2007; Tsoi et al. 2010). One notable observation was that during BB treatment, bimodal peaks were converted into single peaks in the SDN, indicating that the larger particles were eliminated during the physical treatment.

Fig. 2 Hydrodynamic diameter of the treated RP4 plasmid (Malvern Zetasizer Panalytics, Japan) based on size distribution by number, and % frequency (a) comparison of BB-20, BB-10 vs. N (b) shows N with Mg^{2+}concentration-dependent change in size and its distribution

In the correlogram analysis, a linear shoulder was typically observed with increased length, accompanied by a delayed decay curve and a broader decay range of approximately 2 x 10^3 μs. In addition, the mean count rates

(kcps) were within an acceptable range, from 185 to 475 kcps, with no count rates exceeding 500 kcps. The intercept of the correlogram for the 120 ng/µL samples consistently exceeded 0.77, mostly ranging between 0.88 and 0.99. All these parameters may indicate the presence of large, polydisperse particles, which may be coming from genomic DNA, dust or dirt contamination. However, the absence of number fluctuations in the correlogram, or an erratic baseline typically associated with very large particles (Malvern Panalytical, 2017), rules out dirt contaminants due to a flat zero baseline. Lastly, intensity-based size distribution showed that the relative signal intensities (not shown) did not agree with the rule-of-thumb signal proportionality to the square of the molecular weight (Moore and Cerasoli 2010).

BB treatment for the RP4 resulted in a relatively higher D_H size compared to N, and in good agreement with a previous study on shear-induced denaturation (Folarin et al. 2019; Levy et al. 1999). B-20 (minutes) showed a 2.3-fold increase while a 5-fold increase was recorded in BB-10. SDI comparison also showed the same increase in two test concentrations of 100 and 17 ng/uL.

DLS particle size analysis, also known as photon correlation spectroscopy, is a quick, easy, highly sensitive, and high-throughput technique for characterizing the hydrodynamic sizes of biomolecules as a reflection of Brownian, self-diffusive motions including intramolecular motions. The increase in D_H in BB-pDNA reflects the corresponding decrease in the translational diffusion coefficient from the Stoke's-Einstein relation. The reduced diffusion coefficient was also demonstrated in ethidium bromide intercalation where supercoiled or "interwound" conversions to denatured or "toroidal" structures were observed (Chirico et al. 1990). Denaturation is also a process of a reduced torsional or twisting force which is necessary to maintain the supercoiling (Junier et al. 2023). However, this structural change does not pertain to the complete loss of supercoiling in open circular or linear plasmid forms.

Conversely, the addition of Mg^{2+} at 2 mM caused a 1.4-fold decrease in D_H, followed by a 1.6-fold increase at MT-5, with the highest increase observed at MT-10. This pattern was similarly reflected in the SDI data (Table S1) at a lower concentration. Starting from approximately 70 nm, Mg^{2+} addition led to size increases that were directly proportional to Mg^{2+} concentration, ranging from 88.7 nm up to 248 nm while aggregates formed up to 4 *u*m and showing multi-modal distribution similar to a previous study in the same Mg^{2+}-treatment (Süleymanoğlu 2017).

Mg^{2+}, as a divalent cation, interacts with the DNA structure and may induce three simultaneous effects. The first is a reduction in size due to DNA bending caused by intramolecular attraction (Pehrson 1989). The second effect, occurring at higher cation concentrations, is DNA condensation, where DNA chains collapse into compact molecules (Kankia 2003; Ongkudon et al. 2012; Tongu et al. 2016). Third, aggregate formation forming larger structures (Ceci 2004). Condensation likely did not occur at MT-0.3 or even at the higher concentration of 10 mM. The modest size reduction observed at MT-0.3 is probably due to DNA bending or intramolecular attraction, consistent with prior plasmid characterizations involving Mg^{2+} ions (Süleymanoğlu, 2017).

For the MT-5 and MT-10, the formation of more aggregates may be possible due to the larger sizes. The addition of Mg^{2+} ions promote aggregation by facilitating intermolecular attraction through Mg^{2+}-mediated bridging (Ceci, 2004). Such aggregation usually results in a 5 to 10-fold increase in hydrodynamic size compared to untreated plasmids (Lee et al. 2001), and which is similar to the signal intensity size ratios observed among multiple peaks in the untreated control (N).

Finally, analysis based on the DLVO theory provides a reasonable explanation for the MT-pDNA size aggregation. The addition of cations increases the ionic strength of the solution, thereby reducing the thickness of the Debye length (which is inversely proportional to ionic strength). This reduction allows the electric double layers of particles to overlap, allowing the attractive Van der Waals forces to dominate, favouring the attractive interaction energy, leading to the formation of aggregates (Butt et al. 2013).

3.3 Zeta (ζ) potential

The signature of the structural changes as well as the electrokinetic phenomena of the treated plasmids was captured by their zeta potentials. Fig. 3 shows the ζ potential following the different plasmid treatments for the small plasmid, pBR322 and the larger, RP4. The quality factor (criteria > 1.0) was higher than 1.0, while the conductivity was within the 1-10 (1.95) mS/cm criteria for N with a total count rate range of 748–986 kcps. The zeta potential is a linear correlation with electrophoretic mobility as expressed from the Henry's equation (Eqn. 2).

RP4's N showed the highest negative potential at -36.9 mV while both BB and MT-pDNAs have reduced values at -3.2 mV as the lowest value and -6 mV for MT-10. The untreated N's potential is in good agreement with a typical plasmid's zeta potential which is nearly at -40 mV (Prevette et al. 2007; Tsai et al. 1999). These patterns revealed BB-20 and BB-10 to have a 2.3 and 11.7-fold decrease while MT-2, MT-5 and MT-10 showed 1.5, 3.9 and 6.1-fold concentration-dependent decrease, respectively.

The pBR322 plasmid's potential reached -70 mV which was due to the lower concentration and absence of any salt in water. When added with $Mg^{2+,}$ it revealed similar pattern of decreasing potential. However, a notable difference in BB-5 showed that the potential was not significantly altered in pBR322. In the MT-treated plasmid, both plasmids revealed concentration-dependent decrease in the potential which relates inversely with concentration and as observed in the experiments of Manning (1978) with $MgCl_2$ titration with DNA.

The ζ potential measures the electrostatic potential of the plasmid, which acts as a negatively charged polyelectrolyte in solution which forms an electric double layer (EDL) with counterions in the surrounding medium (Schellman and Stigter 1977; Xu et al. 2007). It also serves as an indicator of particle stability according to the DLVO theory. Without any cation, the potential in N indicates sufficient electrostatic repulsion, good particle dispersion and stability.

Fig. 3 (a) Zeta potential of the treated pBR322 (n = 3) (b) RP4 plasmid Only control sample (N) was measured in duplicate Significant difference by independent sample t-test and one asterisk (*) indicates p value < 0.05 (n = 3) Error bars represent one standard deviation.

Further, this also reflects the charge-screening effect on the plasmid's electric field as well as formation of more aggregates as the potential for both plasmids reached the range of -30 to +30 mM, with the highest negative at – 6 mV (Cherng et al. 1996; Tsai et al. 1999; Valente et al. 2021) at MT-10. Similar progressive decreases in ζ potential have been reported with other salts, including both divalent and trivalent cations (Nial and Subudhi 2024; Ongkudon et al. 2012).

Similar reduction of the ζ potential BB-20 and BB-10 observed as compared to N may be different than MT-pDNA since N and BB-pDNA contains the same ionic strength. Supercoiled forms have been reported to have

409 higher potential than the relaxed, open circular forms, and with an inverse relationship with the D_H diameter
410 (Gaspar et al. 2011; Manning 1978). Polynucleotides such as DNA has both a contour (stretched) length and
411 persistence length which is dependent on bending (angle) characteristics of the polymer. An effective charge
412 spacing, *b*, is expressed as the ratio of this persistence length to the number of phosphate groups. DNA molecules
413 with bent conformations would typically have lower charge spacing as compared to its fully stretch form. This
414 bending or conformational change affects the surface charge density (inversely related to *b*) as defined in the
415 manning condensation parameter (Manning, 1975). Finally, the surface charge density is directly related to the
416 zeta or electric potential of the molecule according to the ionic strength from the Grahame principle equation (Butt
417 et al. 2013). Hence, the increase in the hydrodynamic size of the BB-pDNA may correspond to this decrease in
418 surface charge density and the potential at the slipping plane. For the pBR322, it appears that the BB-treatment of
419 the smaller-sized plasmids may not be sensitive to physical treatment and indicates a size-dependent response.
420 This supports the fluorescence emission of the BB-5 treatment in Fig. 1.
421
422 Overall, the fluorescence spectra, hydrodynamic sizes, and zeta potential measurements have described the
423 structural variations in the plasmid upon treatment. A modest limitation of the characterizations are the differences
424 in BB-treatment time and Mg^{2+} concentration ranges and increments employed across different experimental
425 measurements for both plasmids. But despite the differences, pBR322 are all aligned in BB treatment and slightly
426 in MT-pDNA concentrations. For the RP4, BB-treatments are also in agreement in hydrodynamic properties until
427 transformation. Lastly, observable patterns were determined which were more relevant in the characterization and
428 in interpreting the transformability. Future studies are needed by testing other cations with different valences,
429 various sizes of plasmids, consistent denaturation time and concentration ranges to fully integrate structural,
430 electrokinetic variations in pDNAs transformability as well as to generate significant correlations.
431
432 **3.4 Effect of plasmid treatment on transformation efficiency**
433 Following the characterization of the treated plasmids, the transformation efficiency of the plasmid upon treatment
434 was now evaluated. Essentially, the host cell should have a genotypic-based or environmentally inducible cell
435 competence as a condition for transformation gene transfer. Then, extracellular plasmids or DNA fragments must
436 successfully diffuse across the cell membrane before internalization, replication, and expression. Since the surface
437 of the cell membrane and the DNA both have negative charges (Chen et al. 2020), a key step is to overcome the
438 electrostatic repulsion by charge screening to facilitate contact.

Divalent cations in water, herein added with 30mM of Ca^{2+}, may be adsorbed and induce cell competency (Eqn. 4.4) to cause permeabilization of the outer membranes (Bukau et al. 1985). Simultaneously, pDNAs may form (or without) complexes with cations in water, and from the alkaline earth metal cations, Mg^{2+} forms a stronger binding complex (Eqn. 5) (Ahmad et al. 2003; Friedman and Manning, 1984). These two processes should reduce the electrostatic repulsion (Xie et al. 1992), which yields the uptake of the pDNA leading to the transformed *E. coli* cell (Tra-cell) (Eqn. 4.6).

Equations 4-6: Reversible binding or affinity/ dissociation mechanisms for the host cell and pDNA complex

Ca^{2+} + *E. coli* cell ↔ adsorbed Ca^{2+}● *E. coli* + unbound Ca^{2+} Eqn. (4)

2. Mg^{2+} + pDNA ↔ Mg^{2+}● pDNA complex + unbound Mg^{2+} Eqn. (5)

Adsorbed Ca^{2+}● *E. coli* + Mg^{2+}● pDNA complex ↔ Tra ● cell + Adsorbed Ca^{2+}● *E. coli* + Mg^{2+}● pDNA residual + unbound Mg^{2+}/ Ca^{2+} Eqn. (6)

The TE for the pBR322 and RP4 are shown in Figures 4a and 4b, respectively. In pBR322, TE's were not statistically significant, although MT-3 and MT-5 appears to have higher TE's than MT-1, N and BB-5 by a factor of 1.4-2.8. In contrast, RP4's transformation at MT-100 was 4.2-fold higher than N while BB-5 decreased by 2.4-fold. When tested at 100 mM, MT-100 showed significant increase compared to N. The plasmid treatment validates that its effect is more significant in the larger plasmid as reflected in the transformation. This is in good agreement with a previous study on the effect of shearing on the loss of supercoiling content, which was more pronounced in larger plasmid (~ 29 kb), and with no detectable difference with or without shearing for the smaller, 13 kb (Levy et al. 1999). This reduction of TE may be compared to a decreased frequency of gene transfer within the range of 50-75% reduction of an OC plasmids (or a relaxed plasmid) in reference to a CCC (Hanahan 1983) for a 3kb and 10kb plasmid (Demaneche et al. 2002).

Fig. 4 (a) TE for the pBR322 with the different treatments (b) TE for the RP4. Significant difference by independent sample t-test and one asterisk (*) indicates p value < 0.05 (n = 3) Error bars represent one standard deviation

At MT-100, the drastic increase in TE agrees well with the previous transformation in *P. aeroginosa* with RP4 plasmid (Mercer and Loutit 1979). Further, this may have also been the effect of the Mg^{2+}-induced condensation not captured by D_H or not achieved with a significant reduction of the ζ potential by around 89% (charge neutralization) as a criterion for DNA condensation (Bloomfield 1996). The zeta potential of MT-100 for the RP4 may have progressed towards the positive potential which is typically observed in DNA condensation with significant cation neutralization of the negative phosphate charge (Prevette et al. 2007).

Condensation and aggregation were demonstrated in previous works (Bui and Nguyen 2018; Flock et al. 1996; Gao et al. 2019) with Mg^{2+}. For example, as much as 500 mM high concentration of Mg^{2+} is required for a 25 kb plasmid to achieve a 95.2% ξ potential reduction (Ongkudon et al. 2012). Addition of Mg^{2+} ions in DNA has been long reported to decrease the superhelix diameter when individual molecules were observed in solution (Adrian et al. 1990). Indeed, DNA condensation was observed in an AFM image as a compact branched structure from a random coil (without Mg^{2+}) and with sharp decrease of fluorescence at 100 mM Mg^{2+} (Sun et al. 2002).

Hence, it may be prudently realized that the probability of transformation (Eqn. 4.6) was facilitated by a combined process of binding of Mg^{2+} ions to the plasmid, the screening of the interfacial negative charge (lower zeta potential), and the plasmid condensation prior to diffusion across the cell membrane. This effect is analogous to the transfection mechanisms of gene delivery in eukaryotic cells in which a ligand forms a complex with DNA to screen and generate excess positive charge to interact with the negatively charged cell membrane, to condense the complex for enzymatic protection and enhance transfection frequency (Son et al. 2000). These mechanisms support the efficiency of transformation process described in Eqn. 4.6.

Concurrently, the significant reduction in TE from the BB treatment (BB-5) may be attributed to the gene sequence damage by the denaturation or an effect of the treatment to cause changes in the structure. If there were strand breaks in the antibiotic-resistant gene sections in the RP4 (amp and kan genes), no gene expression is expected.

To rule out this hypothesis, Ct values of the amplified *traG* in RT-qPCR for both N-RP4 and BB-10-RP4 were compared. Table S2 shows no significant changes in Ct values, suggesting that the base pair sequence was intact for both BB and N.

Finally, comparing the different plasmid sizes, TE for the untreated, N, for pBR322 (4.3 kb) was higher than RP4 (60 kb) by about 6-logarithmic difference, 2.16 $x10^8$ CFU/ug vs. 177 CFU/ug for the pBR322 and RP4, respectively. The TE at N for the pBR322 is comparable with the non-UV transformation efficiency of Yoon and others (Yoon et al. 2018) and higher than Umar and others, despite both having used a relatively lower molecular weight plasmid (Umar et al. 2021). This pattern follows the negative linear correlation of transformability with plasmid size from as low as 2 kb to 60 kb (Hanahan 1983). However, the work of Hanahan (1983) revealed no drastic reduction of transformation probability in the high molecular weight plasmid (only at 60 kb), considering that the contour length of a 60 kb plasmid is around 20 *u*m in comparison with the *E. coli*'s dimension of 2 um and even more so with the size of the cell membrane porin channel. This suggests other mechanisms worthy of further investigations.

3.5 Implications in water treatment of pDNAs

The effect of the plasmid treatment in transformation may mimic its natural compaction or condensation inside the host by polyamines (or chromatin in eukaryotic cells), including Mg^{2+} as being the most abundant cations in cells. In light-based treatments, targets may be hidden in these compacted structures which may be attributed to the hypochromic effect (Ke et al. 2010; Tsoi et al. 2010).

Conversely, denatured plasmids might be more susceptible to degradation due to their larger size hence more exposure to the targets. Lastly, the effect on pBR322 at MT-5 reflects typical hard water conditions, while MT-100 for RP4 is more relevant in hypersaline water matrices (Borin et al. 2008; Hernández et al. 2023; Lai et al. 2014; Suzuki et al. 2001). These cation concentrations provide additional challenges in the HGT threat of ABR as well as inducing natural cell competence in transforming microbes.

4. Conclusions

Physico-chemical treatments substantially affect the transformation of multidrug-resistant plasmid DNA in *Escherichia coli.* Both inherent plasmid size and environmental factors that modulate plasmid structure affect transformation efficiency. The larger RP4 plasmid (60 kb) demonstrated greater susceptibility to treatment-induced alterations compared to the smaller pBR322 plasmid (4.6 kb). Bead beating increased the hydrodynamic diameter, indicative of structural disruption, which was accompanied with reduced transformation efficiency. In contrast, elevated Mg^{2+} concentrations, particularly at 100 mM, induced plasmid condensation and a concentration-dependent charge neutralization in enhancing plasmid uptake efficiency. Future studies should investigate the effects of other cationic elements present in water to find new methods of eliminating HGT.

5. References

Adrian, M., Heggeler-Bordier, B. ten, Wahli, W., Stasiak, A., Stasiak, A., & Dubochet, J. (1990). Direct visualization of supercoiled DNA molecules in solution. *The EMBO Journal*, *9*(13), 4551–4554. https://doi.org/10.1002/j.1460-2075.1990.tb07907.x

Ahmad R, Arakawa H, Tajmir-Riahi HA (2003) A Comparative Study of DNA Complexation with Mg (II) and Ca (II) in Aqueous Solution: Major and Minor Grooves Bindings. Biophysical Journal 84(4) 2460–2466. https://doi.org/10.1016/s0006-3495(03)75050-4

Amarasiri M, Sano D, Suzuki S (2019) Understanding human health risks caused by antibiotic-resistant bacteria (ARB) and antibiotic resistance genes (ARG) in water environments: Current knowledge and questions to be answered. Critical Reviews in Environmental Science and Technology 50(19) 1–44. https://doi.org/10.1080/10643389.2019.1692611

Bloomfield VA (1996) DNA condensation. Current Opinion in Structural Biology 6(3) 334–341. https://doi.org/10.1016/s0959-440x(96)80052-2

Bochman, M. L., Paeschke, K., & Zakian, V. A. (2012). DNA secondary structures: stability and function of G-quadruplex structures. *Nature Reviews Genetics*, *13*(11), 770–780. https://doi.org/10.1038/nrg3296

Bui, V.-C., & Nguyen, T.-H. (2018). DNA aggregation induced by Mg2+ ions under different conditions. Journal of Molecular Recognition, 31(9), e2721. https://doi.org/10.1002/jmr.2721

Butt, H.-J., Graf, K., & Kappl, M. (2013). Physics and Chemistry of interfaces. Wiley-Vch Verlag Gmbh.

554 Ceci, P. (2004). DNA condensation and self-aggregation of Escherichia coli Dps are coupled phenomena related
555 to the properties of the N-terminus. *Nucleic Acids Research*, *32*(19), 5935–5944.
556 https://doi.org/10.1093/nar/gkh915
557 Cherng JY, Schuurmans-Nieuwenbroek NME, Jiskoot W, Talsma H, Zuidam NJ, Hennink WE, Crommelin DJA
558 (1999) Effect of DNA topology on the transfection efficiency of poly((2-dimethylamino) ethyl
559 methacrylate)–plasmid complexes. Journal of Controlled Release 60(2-3) 343–353.
560 https://doi.org/10.1016/s0168-3659(99)00089-9
561 Chirico, G., Lunelli, L., & Baldini, G. (1990). Conformation of intercalated DNA plasmids investigated by circular
562 dichroism and dynamic light scattering. Biophysical Chemistry, 38(3), 201–211.
563 https://doi.org/10.1016/0301-4622(90)87002-3
564 Demaneche S, Jocteur Monrozier L, Chapel JP, Simonet P (2002) Influence of plasmid conformation and inserted
565 sequence homology on natural transformation of Acinetobacter sp. HAL (Le Centre Pour La
566 Communication Scientifique Directe) 52(61-69).
567 Dragan, A. I., Pavlovic, R., McGivney, J. B., Casas-Finet, J. R., Bishop, E. S., Strouse, R. J., Schenerman, M. A.,
568 & Geddes, C. D. (2012). SYBR Green I: fluorescence properties and interaction with DNA. Journal of
569 Fluorescence, 22(4), 1189–1199. https://doi.org/10.1007/s10895-012-1059-8
570 Flock, S., Labarbe, R., & Houssier, C. (1996). Dielectric constant and ionic strength effects on DNA precipitation.
571 Biophysical Journal, 70(3), 1456–1465. https://doi.org/10.1016/s0006-3495(96)79705-9
572 Folarin, O., Nesbeth, D., Ward, J. M., & Keshavarz-Moore, E. (2019). Application of Plasmid Engineering to
573 Enhance Yield and Quality of Plasmid for Vaccine and Gene Therapy. Bioengineering, 6(2), 54.
574 https://doi.org/10.3390/bioengineering6020054
575 Gao, T., Zhang, W., Wang, Y., & Yang, G. (2019). DNA Compaction and Charge Neutralization Regulated by
576 Divalent Ions in very Low pH Solution. Polymers, 11(2), 337. https://doi.org/10.3390/polym11020337
577 Georgiou CD, Papapostolou I (2006) Assay for the quantification of intact/fragmented genomic DNA. Analytical
578 Biochemistry 358(2) 247–256. https://doi.org/10.1016/j.ab.2006.07.035
579 Guragain, M., Schmidt, J. W., Bagi, L. K., Paoli, G. C., Kalchayanand, N., & Bosilevac, J. M. (2024). Antibiotic
580 Resistance and Disinfectant Resistance Among Escherichia coli Isolated During Red Meat Production.
581 Journal of Food Protection, 87(6), 100288–100288. https://doi.org/10.1016/j.jfp.2024.100288

582 Guéroult, M., Boittin, O., Mauffret, O., Etchebest, C., & Hartmann, B. (2012). Mg2+ in the Major Groove
583 Modulates B-DNA Structure and Dynamics. PLoS ONE, 7(7), e41704.
584 https://doi.org/10.1371/journal.pone.0041704
585 Hahn, M. B. (2025). Rapid quantitative analysis of double-stranded plasmid DNA with capillary gel
586 electrophoresis for applications in quality control and radiation research. Scientific Reports, 15(1).
587 https://doi.org/10.1038/s41598-025-85132-w
588 Hanahan, D., Jessee, J., & Bloom, F. R. (1991). [4] Plasmid transformation of Escherichia coli and other bacteria.
589 Methods in Enzymology, 63–113. https://doi.org/10.1016/0076-6879(91)04006-a
590 Hanahan D (1983) Studies on transformation of Escherichia coli with plasmids. Journal of Molecular Biology
591 166(4) 557–580. https://doi.org/10.1016/s0022-2836(83)80284-8
592 Hershey, A. D., Goldberg, E., Burgi, E., & Ingraham, L. (1963). Local denaturation of DNA by shearing forces
593 and by heat. Journal of Molecular Biology, 6(3), 230–243. https://doi.org/10.1016/s0022-2836(63)80072-
594 8
595 Huang, X., & Chen, X. (1990). Supercondensed structure of plasmid pBR322 DNA in an Escherichia coli DNA
596 topoisomerase II mutant. Journal of Molecular Biology, 216(2), 195–199. https://doi.org/10.1016/s0022-
597 2836(05)80306-7
598 Hur JH, Lee A, Yoo WK, Lee J, Kim, KK (2019) Identification of a new Z-DNA inducer using SYBR green 1 as
599 a DNA conformation sensor. FEBS Letters 593(18) 2628–2636. https://doi.org/10.1002/1873-3468.13513
600 Junier, I., Ghobadpour, E., Espeli, O., & Everaers, R. (2023). DNA supercoiling in bacteria: state of play and
601 challenges from a viewpoint of physics based modeling. *Frontiers in Microbiology*, *14*.
602 https://doi.org/10.3389/fmicb.2023.1192831
603 Kankia BI (2003) Binding of Mg2+ to single-stranded polynucleotides: hydration and optical studies. Biophysical
604 Chemistry 104(3) 643–654. https://doi.org/10.1016/s0301-4622(03)00125-x
605 Kawano, H., Suzuki-Minakuchi, C., Sugiyama, D., Watanabe, N., Takahashi, Y., Okada, K., & Nojiri, H. (2020).
606 A Novel Small RNA on the Pseudomonas putida KT2440 Chromosome Is Involved in the Fitness Cost
607 Imposed by IncP-1 Plasmid RP4. Frontiers in Microbiology, 11. https://doi.org/10.3389/fmicb.2020.01328
608 Ke F, Luu YK, Hadjiargyrou M, Liang D (2010) Characterizing DNA Condensation and Conformational Changes
609 in Organic Solvents. PLoS ONE 5(10) e13308. https://doi.org/10.1371/journal.pone.0013308

610 Kolbeck, P. J., Tišma, M., Analikwu, B. T., Vanderlinden, W., Dekker, C., & Lipfert, J. (2023). Supercoiling-
611 dependent DNA binding: quantitative modeling and applications to bulk and single-molecule experiments.
612 Nucleic Acids Research, 52(1), 59–72. https://doi.org/10.1093/nar/gkad1055
613 Krause, S., Pansegrau, W., Lurz, R., de la Cruz, F., & Lanka, E. (2000). Enzymology of Type IV Macromolecule
614 Secretion Systems: the Conjugative Transfer Regions of Plasmids RP4 and R388 and the cag Pathogenicity
615 Island of Helicobacter pylori Encode Structurally and Functionally Related Nucleoside Triphosphate
616 Hydrolases. Journal of Bacteriology, 182(10), 2761–2770. https://doi.org/10.1128/jb.182.10.2761-
617 2770.2000
618 Lai, K.-C., Chen, J.-W., Chen, W.-T., Wan, T.-J., Wen, J.-C., & Shu, C.-M. (2014). Applications of the Taguchi
619 Method for Key Parameter Screening in Electrodialysis Reversal Used for High Salinity Wastewater.
620 CLEAN–- Soil, Air, Water, 42(12), 1751–1758. https://doi.org/10.1002/clen.201300169
621 Levy, M. S., Collins, I. J., Yim, S. S., Ward, J. M., Titchener-Hooker, N., Ayazi Shamlou, P., & Dunnill, P. (1999).
622 Effect of shear on plasmid DNA in solution. Bioprocess Engineering, 20(1), 7.
623 https://doi.org/10.1007/s004490050552
624 Liu, Y., Wang, P., Dou, S., Zhang, W., Wang, X., & Sang, H. (2011). Monitoring the binding of metal cations
625 and histones to DNA in real time using fluorescence assays. Chinese Science Bulletin, 56(11), 1080–1085.
626 https://doi.org/10.1007/s11434-011-4393-3
627 Manaia CM (2017) Assessing the Risk of Antibiotic Resistance Transmission from the Environment to Humans:
628 Non-Direct Proportionality between Abundance and Risk. Trends in Microbiology 25(3) 173–181.
629 https://doi.org/10.1016/j.tim.2016.11.014
630 Manning, G. S. (1977). Limiting laws and counterion condensation in polyelectrolyte solutions. Biophysical
631 Chemistry, 7(2), 95–102. https://doi.org/10.1016/0301-4622(77)80002-1
632 Manning, G. S. (1978). The molecular theory of polyelectrolyte solutions with applications to the electrostatic
633 properties of polynucleotides. Quarterly Reviews of Biophysics, 11(2), 179–246.
634 https://doi.org/10.1017/S0033583500002031
635 Moore, J. D., & Cerasoli, E. (2010). Particle Light Scattering Methods and Applications (pp. 2077–2088).
636 https://doi.org/10.1016/B978-0-12-374413-5.00040-3
637 Nath K, Sarosy JW, Hahn J, Di Como CJ (2000) Effects of ethidium bromide and SYBR® Green I on different
638 polymerase chain reaction systems. Journal of Biochemical and Biophysical Methods 42(1) 15–29.
639 https://doi.org/10.1016/S0165-022X(99)00033-0

Nayvelt, I., Thomas, T., & Thomas, T. J. (2006c). Mechanistic Differences in DNA Nanoparticle Formation in the Presence of Oligolysines and Poly-l-lysine. *Biomacromolecules*, *8*(2), 477–484. https://doi.org/10.1021/bm0605863

Nial, P. S., & Subudhi, U. (2024). Zeta potential of Z-DNA: A new signature to study B-Z transition in linear and branched DNA. International Journal of Biological Macromolecules, 266, 131238–131238. https://doi.org/10.1016/j.ijbiomac.2024.131238

Ongkudon CM, Hodges E, Murphy K, Danquah MK (2012) Removal of endotoxins from plasmid DNA: Analysis of aggregative interaction of mobile divalent metal cations with endotoxins and plasmid DNA. Journal of Separation Science 35(22) 3208–3216. https://doi.org/10.1002/jssc.201200237

Pehrson, J. R. (1989). Thymine dimer formation as a probe of the path of DNA in and between nucleosomes in intact chromatin. Proceedings of the National Academy of Sciences, 86(23), 9149–9153. https://doi.org/10.1073/pnas.86.23.9149

Prevette LE, Kodger TE, Reineke TM, Lynch ML (2007) Deciphering the Role of Hydrogen Bonding in Enhancing pDNA−Polycation Interactions. Langmuir 23(19) 9773–9784. https://doi.org/10.1021/la7009995

Rouzina, I., & Bloomfield, V. A. (1998). DNA Bending by Small, Mobile Multivalent Cations. Biophysical Journal, 74(6), 3152–3164. https://doi.org/10.1016/s0006-3495(98)78021-x

Sandhu, L. C., Warters, R. L., & Dethlefsen, L. A. (1985). Fluorescence studies of Hoechst 33342 with supercoiled and relaxed plasmid pBR322 DNA. Cytometry, 6(3), 191–194. https://doi.org/10.1002/cyto.990060304

Schellman JA, Stigter D (1977) Electrical double layer, zeta potential, and electrophoretic charge of double-stranded DNA. Biopolymers 16(7) 1415–1434. https://doi.org/10.1002/bip.1977.360160704

Shapiro, A. B., Jahić, H., Prasad, S., Ehmann, D. E., Thresher, J., Gao, N., & Hajec, L. I. (2010). A Homogeneous, High-Throughput Fluorescence Anisotropy-Based DNA Supercoiling Assay. SLAS DISCOVERY, 15(9), 1088–1098. https://doi.org/10.1177/1087057110378624

Sun, X.-G., Cao, E.-H., Zhang, X., Liu, D., & Bai, C. (2002). The divalent cation-induced DNA condensation studied by atomic force microscopy and spectra analysis. Inorganic Chemistry Communications, 5(3), 181–186. https://doi.org/10.1016/s1387-7003(02)00320-9

Suzuki, K., Tanaka, Y., Osada, T., & Waki, M. (2001). Concentrations of Phosphorous, Magnesium and Calcium in Swine Wastewater and Possibility of Removing These Components through Crystallization. Nihon Chikusan Gakkaiho, 72(1), 72–79. https://doi.org/10.2508/chikusan.72.72

Szostková, M., & Horáková, D. (1998). The effect of plasmid DNA sizes and other factors on electrotransformation of Escherichia coli JM109. Bioelectrochemistry and Bioenergetics, 47(2), 319–323. https://doi.org/10.1016/s0302-4598(98)00203-7

Süleymanoğlu, E. (2017). Mg2+-induced DNA compaction, condensation, and phase separation in gene delivery vehicles based on zwitterionic phospholipids: a dynamic light scattering and surface-enhanced Raman spectroscopic study. JBIC Journal of Biological Inorganic Chemistry, 22(8), 1165–1177. https://doi.org/10.1007/s00775-017-1492-x

Tongu C, Kenmotsu T, Yoshikawa Y, Zinchenko A, Chen N, Yoshikawa K (2016) Divalent cation shrinks DNA but inhibits its compaction with trivalent cation. The Journal of Chemical Physics 144(20) 205101. https://doi.org/10.1063/1.4950749

Tsai, J. T., Keshavarz-Moore, E., Ward, J. M., Hoare, M., Ayazi Shamlou, P., & Dunnill, P. (1999). Characterisation of plasmid DNA conjugates as a basis for their processing. Bioprocess Engineering, 21(3), 279–279. https://doi.org/10.1007/s004490050676

Tsoi M, Trinh T, Tang VJ, Aguilera J, Perry CC, Milligan JR (2010) Characterization of condensed plasmid DNA models for studying the direct effect of ionizing radiation. Biophysical Chemistry 147(3) 104–110. https://doi.org/10.1016/j.bpc.2009.12.006

Valente, J. F. A., Pereira, P., Sousa, A., Queiroz, J. A., & Sousa, F. (2021). Effect of Plasmid DNA Size on Chitosan or Polyethyleneimine Polyplexes Formulation. Polymers, 13(5), 793. https://doi.org/10.3390/polym13050793

von Wintersdorff CJH, Penders J, van Niekerk JM, Mills ND, Majumder S, van Alphen LB, Savelkoul PHM, Wolffs PFG (2016) Dissemination of Antimicrobial Resistance in Microbial Ecosystems through Horizontal Gene Transfer. Frontiers in Microbiology 7(173). https://doi.org/10.3389/fmicb.2016.00173

Wang Z, Yang Y, Gomes MP, Suthar S (2022) Antibiotics and Antibiotic Resistance Genes in Waters: Pollution, Risks, and Control. Frontiers Media SA.

Xu, R., Wu, C., & Xu, H. (2007). Particle size and zeta potential of carbon black in liquid media. Carbon, 45(14), 2806–2809. https://doi.org/10.1016/j.carbon.2007.09.010

Yoon, Y., Dodd, M. C., & Lee, Y. (2018). Elimination of transforming activity and gene degradation during UV and UV/H2O2 treatment of plasmid-encoded antibiotic resistance genes. Environmental Science: Water Research & Technology, 4(9), 1239–1251.

699 Zinchenko AA, Sakai H, Matsuoka S, Murata S (2009) Application of DNA condensation for removal of mercury
700 ions from aqueous solutions. Journal of Hazardous Materials 168(1) 38–43.
701 https://doi.org/10.1016/j.jhazmat.2009.01.121
702 Zipper H, Brunner H, Bernhagen J, Vitzthum F (2004) Investigations on DNA intercalation and surface binding
703 by SYBR Green I, its structure determination and methodological implications. Nucleic Acids Research
704 32(12) e103. https://doi.org/10.1093/nar/gnh101
705
706
707 **Acknowledgments**
708 This work was supported by the Japan Society for the Promotion of Science (JSPS) Grants-in-Aid for Scientific
709 Research (A) (20H00257). The authors acknowledge the PhD research supervision of Professor Kumiko Oguma
710 to Achilles E. Espaldon during the latter's PhD studies at the University of Tokyo. Also, the main author
711 acknowledge the financial support for the PhD scholarship (Achilles Espaldon) from the Philippine's Department
712 of Science and Technology, Science and Education Institute (DOST-SEI) under Dr. Josette T. Biyo, Ph.D. The
713 authors also acknowledge Prof. Hideaki Nojiri, Ph.D., and Assoc. Prof. Chiho Suzuki-Minakuchi, Ph.D. of the
714 Laboratory of Environmental Biochemistry, Agro-Biotech Research Center (AgTECH), Graduate School of
715 Agricultural and Life Sciences, The University of Tokyo, for the donation of the plasmids. In addition, the authors
716 also would like to thank the Biotech Laboratory of the West Visayas State University, Iloilo City, Philippines, for
717 the fluorescence measurements. For the main author's dissertation committee in which this research article was
718 part of the manuscript, acknowledgements to to Professor Kumiko OGUMA (Chairperson), Professor Hiroyuki
719 KATAYAMA (both from the University of Tokyo), Professor Toru WATANABE (Yamagata University),
720 Associate Professor Ikuro KASUGA, and Associate Professor Tomohiro TOBINO (both from the University of
721 Tokyo).
722
723
724 **Funding**
725 This work was supported by the Japan Society for the Promotion of Science (JSPS) Grants-in-Aid for Scientific
726 Research (A) (20H00257).
727
728

Authorship contribution statement

The main author, Achilles E. Espaldon did the conceptualization, data curation, formal analysis, methodology, software, supervision, visualization, validation, writing of the original draft as well as the review & editing. Stephen G. Sabinay contributed the methodology, data curation, resources and review and manuscript editing. Ignacio A. Catelo and Noel Peter B. Tan performed the review and editing.

Ethical Approval

This is not applicable

Consent to Participate

This is not applicable

Consent to Publish

This is not applicable

Competing Interest

The authors declare that they have no known competing financial interests or personal relationships that could have appeared to influence the work reported in this paper.

Data Availability Statement

Data available on request from the authors

Figures

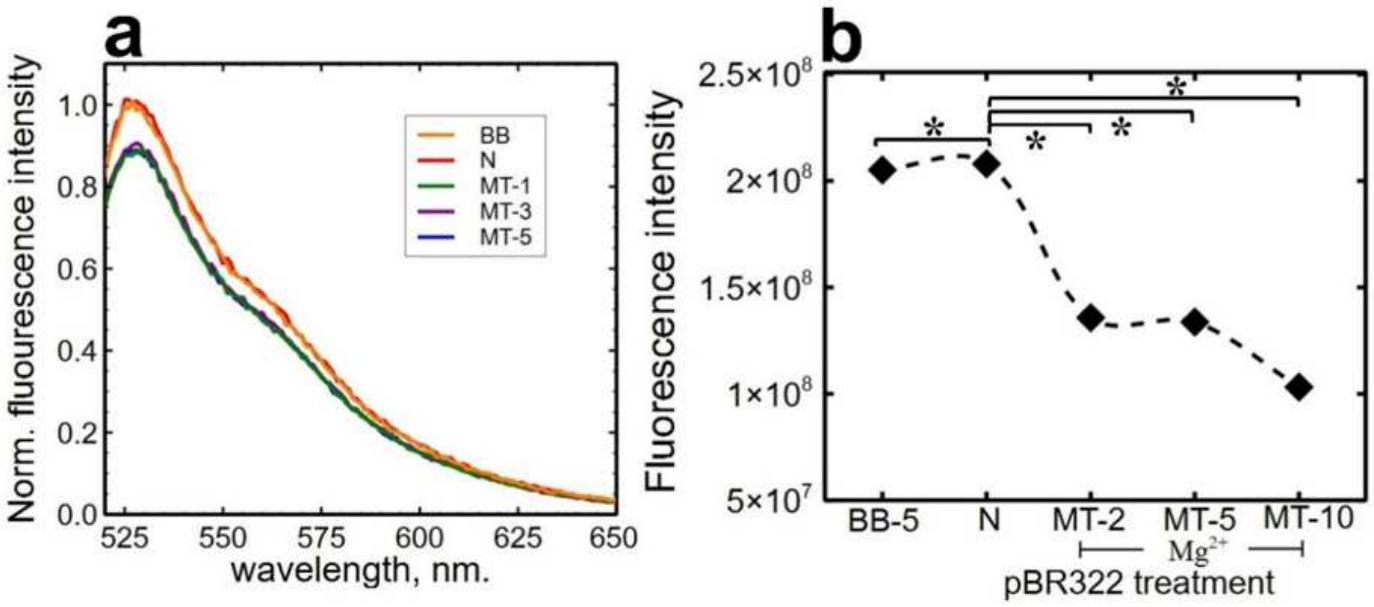


Figure 1

(a) Fluorescence spectra of pBR322 upon treatment (b) End-point fluorescence emission at 530 nm (n = 3). Significant difference by independent sample t-test and one asterisk (*) indicates p value < 0.05 (n = 3). Error bar (not seen due to minimal deviation relative to intensity) is one standard deviation.

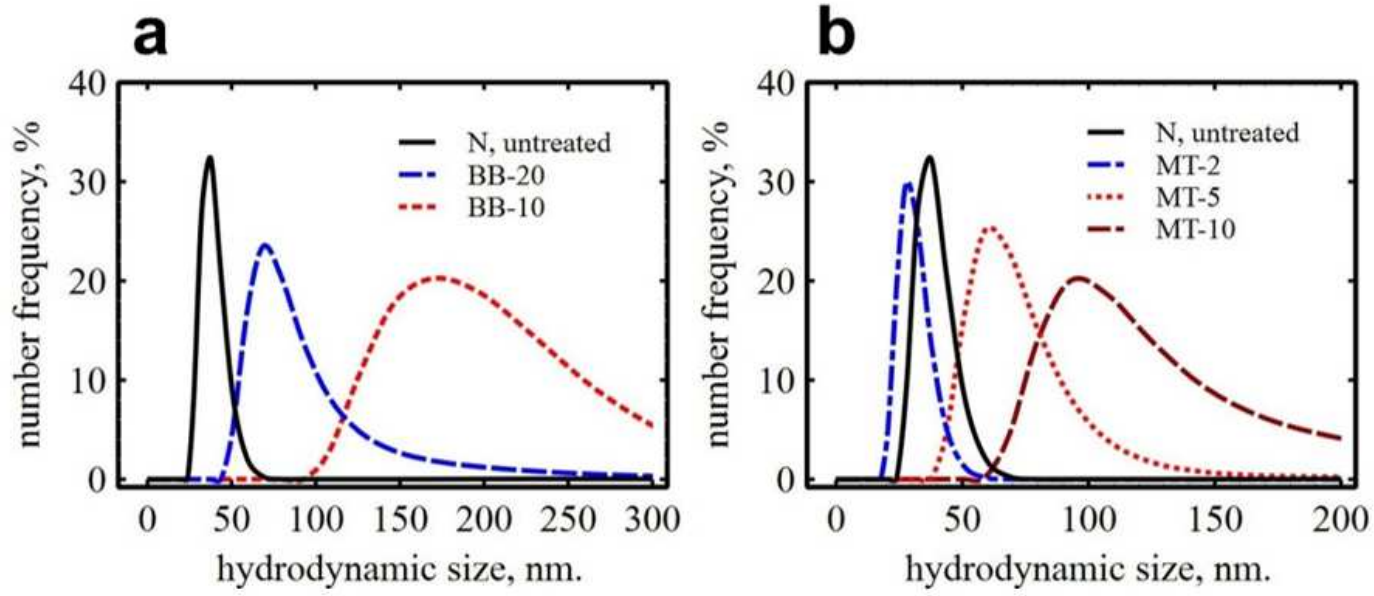


Figure 2

Hydrodynamic diameter of the treated RP4 plasmid (Malvern Zetasizer Panalytics, Japan) based on size distribution by number, and % frequency (a) comparison of BB-20, BB-10 vs. N (b) shows N with Mg^{2+}concentration-dependent change in size and its distribution

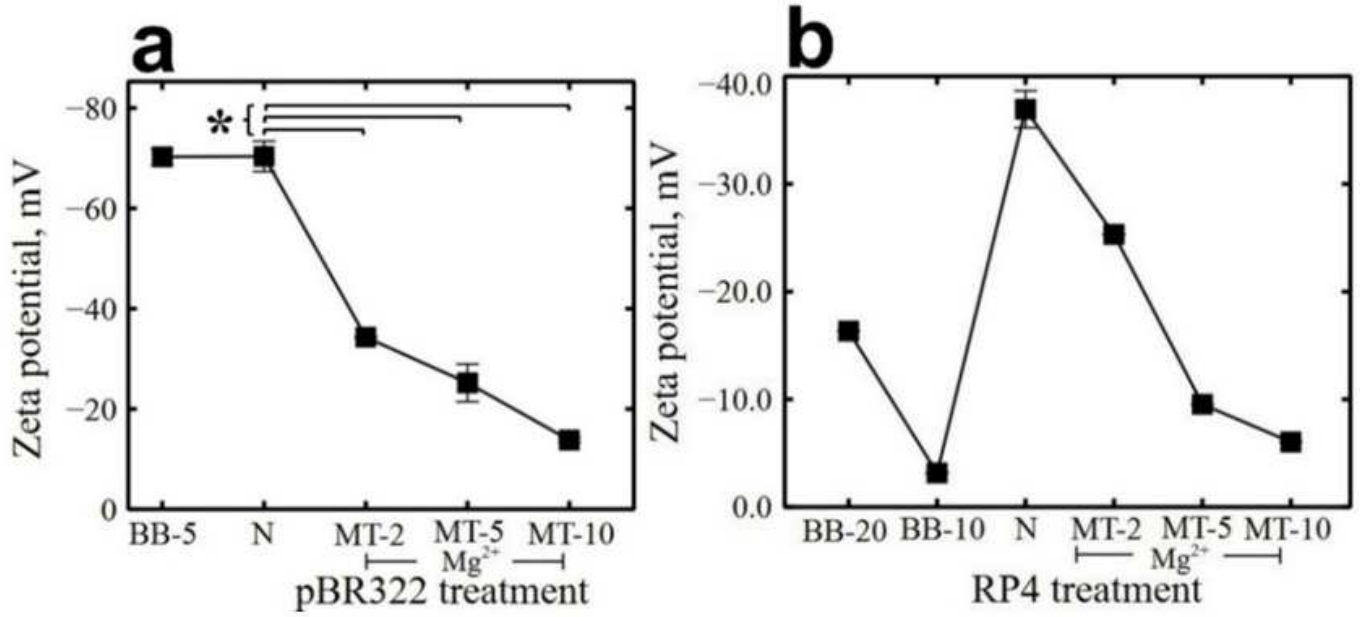


Figure 3

(a) Zeta potential of the treated pBR322 (n = 3) (b) RP4 plasmid Only control sample (N) was measured in duplicate Significant difference by independent sample t-test and one asterisk (*) indicates p value < 0.05 (n = 3) Error bars represent one standard deviation.

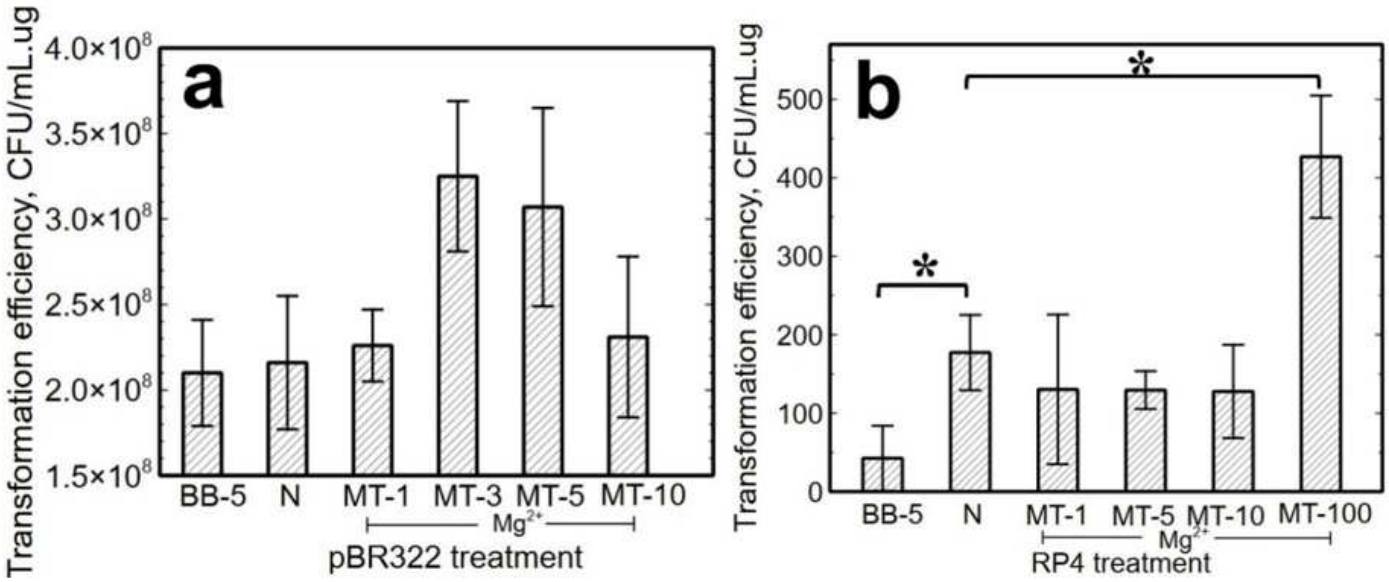


Figure 4

(a) TE for the pBR322 with the different treatments (b) TE for the RP4. Significant difference by independent sample t-test and one asterisk (*) indicates p value < 0.05 (n = 3). Error bars represent one standard deviation

Supplementary Files

This is a list of supplementary files associated with this preprint. Click to download.

- GraphicalAbstract.png
- HydrodynamicvariationsofplasmidDNASupp.docx
- Table1.docx